Transformation Optics Approach to Plasmon-Exciton Strong Coupling in Nanocavities
– *Supplemental Material* –

Rui-Qi Li,[1,2] D. Hernangómez-Pérez,[1] F. J. García-Vidal,[1,3] and A. I. Fernández-Domínguez[1]

[1]*Departamento de Física Teórica de la Materia Condensada and Condensed Matter Physics Center (IFIMAC), Universidad Autónoma de Madrid, E-28049 Madrid, Spain*

[2]*Key Laboratory of Modern Acoustics, MOE, Institute of Acoustics, Department of Physics, Nanjing University, Nanjing 210093, People's Republic of China*

[3]*Donostia International Physics Center (DIPC), E-20018 Donostia/San Sebastián, Spain*

I. TRANSFORMATION OPTICS: 3D GENERALIZED INVERSION

In order to study the [quantum] dynamical properties of single quantum emitters placed in nanometric size metallic cavities supporting localized surface plasmon-polariton (SP) modes we use transformation optics, a powerful and intuitive technique successfully applied in the field of nano-optics in recent years (see recent reviews in Refs. [1]-[2]). This theoretical approach will allow us to obtain insightful analytical expressions for the spectral density and spatial profile of hybrid plasmon-exciton-polariton (PEP) modes in the quasi-static limit. As mentioned in the main text, we will assume that the electric and magnetic fields are decoupled, *i.e.* $\boldsymbol{\nabla}_{\mathbf{r}} \times \mathbf{E}(\mathbf{r}) = \mathbf{0}$, since the dimer size is much smaller than the quantum emitter characteristic wavelength $\lambda_{\rm E} = 2\pi c/\omega_{\rm E}$. The present scheme provides as well an efficient computational framework valuable in the thorough numerical study of the quantum dynamical properties of PEPs at the single emitter level in metallic cavities with non-trivial Gaussian curvature, taking also into account the lossy character of the SP excitations.

To begin with, we consider the generalized inversion based on Ref. [3], noted as $\mathcal{J}$, and defined by

$$\boldsymbol{\varrho}' = \frac{R_T^2}{(z-z_0)^2+\varrho^2}\,\boldsymbol{\varrho}, \tag{1a}$$

$$z' - z_0' = -\frac{R_T^2}{(z-z_0)^2+\varrho^2}\,(z-z_0). \tag{1b}$$

Here, the non-primed variables describe the original frame (with inversion point $\mathbf{z}_0 = z_0\hat{\mathbf{z}}$), the primed variables correspond to the transformed space (with inversion point $\mathbf{z}_0' = z_0'\hat{\mathbf{z}}$), and R_T^2 is an arbitrary length scale. We also define $\boldsymbol{\varrho} = (x, y)$ so that $\mathbf{r} = (\boldsymbol{\varrho}, z)$ (and similarly for the primed variables). Note the additional $-$ sign in Eq. (1b) compared to the inversion transformation used in Refs. [4]-[5] which yields $z_0' > 0$ (we fix by construction $z_0 > 0$).

Being a member of the family of inversion transformations in three-dimensional Euclidean spaces, the mapping given by Equations (1a)-(1b) transforms the infinity in a given reference frame to the inversion point in the other reference frame. It also maps a pair of metallic spheres, of radii R_1 and R_2 (see the left panel of Fig. I) into a system of two concentric spheres centered at the origin of coordinates: an inner solid sphere, of radius R_1', and a hollow outer sphere, of radius R_2' (see right panel of Fig. I). The gap between the spheres in the original frame, where the quantum emitter is located (*i.e.* $R_2 \leq R_2 + z_{\rm E} \leq R_2 + \delta$) is mapped within the annulus region between the transformed concentric spheres at positions far away from the inversion point.

For the transformation from the coordinate frame $\mathbf{r} \to \mathbf{r}' = \mathbf{r}'(\mathbf{r}) = \mathcal{J}\,\mathbf{r}$ to preserve Maxwell's equations (or, in the long wavelength limit used here, Laplace equation) the components of the dielectric permittivity tensor must necessarily verify the general relation [2]

$$\epsilon'_{\alpha',\beta'}(\mathbf{r}',\omega) = \frac{1}{\det \mathbb{J}_{\mathbf{r}'}} \sum_{\alpha,\beta} (\mathbb{J}_{\mathbf{r}'})_{\alpha',\alpha} (\mathbb{J}_{\mathbf{r}'})_{\beta',\beta} \epsilon_{\alpha,\beta}[\mathbf{r}(\mathbf{r}'),\omega], \tag{2}$$

where $(\mathbb{J}_{\mathbf{r}'})_{\alpha,\alpha'} = \partial \mathbf{r}_\alpha / \partial \mathbf{r}'_{\alpha'}$ is the Jacobian matrix of the transformation. Note that Eq. (2) implies that, if in the original coordinate system the metallic spheres and the dielectric medium are spatially homogeneous, the full system becomes inhomogeneous in the transformed frame. Fortunately, this fact does not introduce additional complications in the scattering problem for the electrostatic potential $\Phi'(\mathbf{r}') = \Phi[\mathbf{r}'(\mathbf{r})]$ since application of the electromagnetic (EM) boundary conditions for the Laplace equation in each region of the transformed space trivially removes any spatially dependent factor.

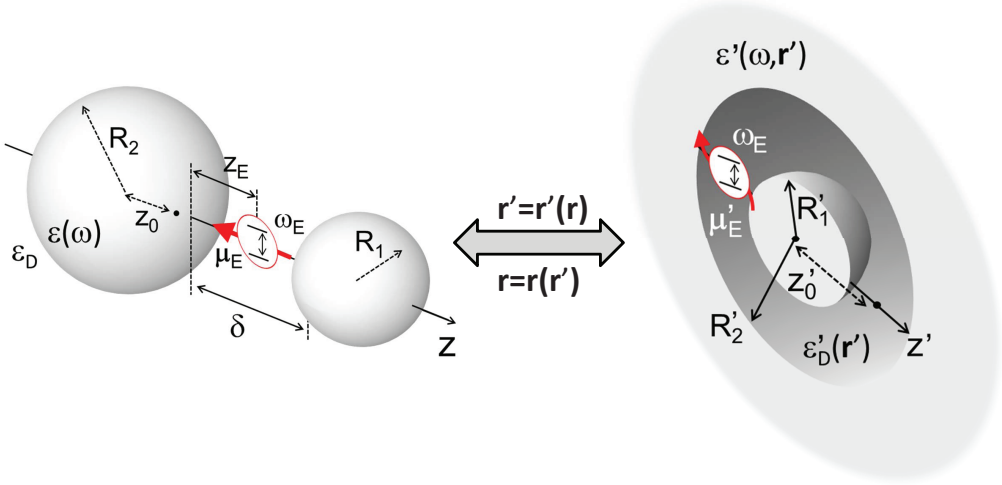

FIG. I: Sketch of the inversion transformation that maps an spherical dimer nanocavity (left) into a concentric annulus geometry (right), and vice versa. Note that the right panel shows a cross sectional view of the transformed geometry. The mapping also modifies the original permittivities, which acquire an spatial dependence in the annulus frame given by Eq. (2). The dipole source modelling the emitter is also affected by the mapping, and its primed counterpart can be expressed in the form of Eq. (3). Importantly, the transformation does not alter the spectral characteristics of the original system.

II. GENERAL SOLUTION TO THE SCATTERING PROBLEM

Our strategy to obtain the EM Green's function $\mathbb{G}(\mathbf{r},\mathbf{r}',\omega)$, which describes the EM properties of the full system (single emitter and plasmonic metallic dimer of radii R_i, with $i \in \{1,2\}$ and gap δ) is to take into account that the transformation given in Eqs. (1a)-(1b) is still an inversion. Then, it is well known (see Refs. [4], [5]) that the electrostatic potential has to be forcefully written as $\Phi'(\mathbf{r}') = |\mathbf{r}' - \mathbf{z}'_0|\tilde{\Phi}'(\mathbf{r}')$ where $\tilde{\Phi}'(\mathbf{r}')$ is solution of Laplace equation in the new transformed space, $\Delta_{\mathbf{r}'}\tilde{\Phi}'(\mathbf{r}') = 0$. If the source is located on the $\hat{\mathbf{z}}$ axis and oriented towards the same direction, $\boldsymbol{\mu}_{\mathrm{E}} = \mu_{\mathrm{E}}\hat{\mathbf{z}}$, the physical system is rotationally invariant around that axis and we can express $\tilde{\Phi}'(\mathbf{r}')$ as a sum of harmonic modes having the $\hat{\mathbf{z}}$ projection of the angular momentum $m = 0$

$$\tilde{\Phi}'(\mathbf{r}') = \sum_{l=0}^{+\infty}\left[c_l^1\left(\frac{r'}{z'_0}\right)^{l} + c_l^2\left(\frac{r'}{z'_0}\right)^{-(l+1)}\right]Y_{l,0}(\theta',\varphi') \tag{3}$$

with $\mathbf{r} = (r',\theta',\varphi')$ being the position vector expressed in spherical coordinates and $Y_{l,0}(\theta',\varphi')$ the usual spherical harmonics. From a practical point of view, the infinite series is made finite by imposing a cut-off value of the orbital angular momentum, $l \in [0, l_{\max}]$, taking into account the convergence properties of Laplace expansions. The electrostatic potential is now written as the combination of the source and scattered components, $\tilde{\Phi}'(\mathbf{r}') = \tilde{\Phi}'_s(\mathbf{r}') + \tilde{\Phi}'^{\,\mathrm{sc}}(\mathbf{r}')$, and the unknown scattering coefficients in each region are obtained by means of the reflection matrix, $\mathbb{R}$, once the dipolar source is expanded also in harmonic modes. The latter matrix relates the scattering coefficients to the source coefficients by means of the matrix relation $\mathbf{c}^{\mathrm{sc}} = \mathbb{R}\,\mathbf{c}_s$ where $\mathbf{c}^{\mathrm{sc}}$ and $\mathbf{c}_s$ are block column vectors containing the coefficients of the harmonic expansion in Eq. (3).

An essential step in our approach is thus to obtain the reflection matrix, defined as $\mathbb{R} := \mathbb{T}^{-1}\mathbb{S}$, where $\mathbb{T}$ and $\mathbb{S}$ are, respectively, the scattering and source matrices. The latter are built from the application of the EM boundary conditions for the electric and displacement fields in the annulus frame. The scattering matrix can be written in block form

$$\mathbb{T} = \begin{pmatrix} \mathbb{T}_{11} & \mathbb{T}_{12} \\ \mathbb{T}_{21} & \mathbb{T}_{22} \end{pmatrix}, \tag{4}$$

where each of the blocks $\mathbb{T}_{ij}$ is a tridiagonal matrix of dimension $(l_{\max}+1)\times(l_{\max}+1)$. In addition, it can be easily checked that for a source located in the gap, the $\mathbb{S}$ matrix is block diagonal, $\mathbb{S} = \mathbb{S}_{ij}\,\delta_{i,j}$, with matrix elements related

to the $\mathbb{T}$ matrix by means of the relation $\mathbb{S}_{ij} = -\mathbb{T}_{ij}$. The scattering matrix elements are given by

$$\begin{aligned}
\mathbb{T}_{11}(l,l') &= -\delta_{l,l'}\left[(l+1)r_1^{'2}+l\right]r_1^{'l} \\
&\quad + (2l'+1)r_1^{'l'+1}\Big[A_+(l'+1)\delta_{l,l'+1} + A_-(l'+1)\delta_{l,l'-1}\Big], \qquad (5a)\\
\mathbb{T}_{12}(l,l') &= \delta_{l,l'}\left\{\frac{r_1^{'2}-1}{\tilde{\epsilon}(\omega)-1} - \left[(l+1)r_1^{'2}+l\right]\mathrm{e}^{\alpha(\omega)}\right\}r_1^{'-(l+1)} \\
&\quad + \mathrm{e}^{\alpha(\omega)}(2l'+1)r_1^{'-l'}\Big[A_+(l'+1)\delta_{l,l'+1} + A_-(l'+1)\delta_{l,l'-1}\Big], \qquad (5b)\\
\mathbb{T}_{21}(l,l') &= \delta_{l,l'}\left\{\frac{r_2^{'2}-1}{\tilde{\epsilon}(\omega)-1} - \left[lr_2^{'2}+(l+1)\right]\mathrm{e}^{\alpha(\omega)}\right\}r_2^{'l} \\
&\quad - \mathrm{e}^{\alpha(\omega)}(2l'+1)r_2^{'l'+1}\Big[A_+(l'+1)\delta_{l,l'+1} + A_-(l'+1)\delta_{l,l'-1}\Big], \qquad (5c)\\
\mathbb{T}_{22}(l,l') &= \delta_{l,l'}\left[l\,r_2^{'2}+(l+1)\right]r_2^{'-(l+1)} \\
&\quad - (2l'+1)r_2^{'-l'}\Big[A_+(l'+1)\delta_{l,l'+1} + A_-(l'+1)\delta_{l,l'-1}\Big]. \qquad (5d)
\end{aligned}$$

together with the auxiliary functions

$$A_+(l) = \sqrt{\frac{(l+1)^2}{(2l+1)(2l+3)}}, \qquad (6a)$$

$$A_-(l) = \sqrt{\frac{l^2}{(2l-1)(2l+1)}}. \qquad (6b)$$

Note that we have defined the reduced permittivity $\tilde{\epsilon}(\omega) := \epsilon(\omega)/\epsilon_{\mathrm{D}}$ in Eqs. (5a)-(5d). This corresponds to the ratio between the permittivity of the metallic spheres, $\epsilon(\omega)$, and the permittivity of the dielectric medium in which they are embedded, ϵ_{D}. As mentioned in the main text, the EM response of the metal is described by means of a local Drude response function

$$\epsilon(\omega) = \epsilon_\infty - \frac{\omega_{\mathrm{p}}^2}{\omega(\omega+i\gamma)}, \qquad (7)$$

where ε_∞ is the high-frequency offset, ω_{p} the plasma frequency of the electron gas and Ohmic losses are taken into account through the Drude damping parameter γ (we consider silver nanospheres with $\epsilon_\infty = 4.6$, $\omega_{\mathrm{p}} = 9$ eV and $\gamma = 0.1$ eV, see Ref. [9]). From the reduced permittivity, we also define the function

$$\mathrm{e}^{\alpha(\omega)} := \frac{\tilde{\epsilon}(\omega)+1}{\tilde{\epsilon}(\omega)-1}. \qquad (8)$$

For practical purposes, it also convenient to express the reduced radii $r_i' = R_i'/z_0'$ for $i \in \{1,2\}$ in terms of variables which are defined in the original frame only. After some algebra using Eqs. (1a)-(1b) we get

$$r_1' = \frac{1-\tilde{\Delta}_1}{1+\tilde{\Delta}_1}, \qquad (9a)$$

$$r_2' = \frac{1+\tilde{\Delta}_2}{1+\tilde{\Delta}_1}, \qquad (9b)$$

where

$$\tilde{\Delta}_1 := \frac{\delta+d}{2R_1+\delta+d}, \qquad (10a)$$

$$\tilde{\Delta}_2 := \frac{\delta}{d} + \frac{\delta+d}{2R_2-d}, \qquad (10b)$$

Here $d = R_2 - z_0$, and the inversion point, z_0, is related to geometrical parameters of the spherical dimer by the relation

$$z_0 = \frac{(R_1+R_2+\delta)^2 + R_2^2 - R_1^2 - \sqrt{\delta(\delta+2R_1)(\delta+2R_2)(2R_1+2R_2+\delta)}}{2(R_1+R_2+\delta)}. \tag{11}$$

Finally, knowledge of the scattering coefficients allows us to write the scattered electrostatic potential in the quasi-static limit and, as a consequence, the scattered electric field $\mathbf{E}^{\rm sc}(\mathbf{r}) = \boldsymbol{\nabla}_{\mathbf{r}}\Phi^{\rm sc}(\mathbf{r}) = \boldsymbol{\nabla}_{\mathbf{r}}\Phi^{'\,\rm sc}[\mathbf{r}'(\mathbf{r})]$ and the corresponding EM Green's function, $\mathbb{G}^{\rm sc}(\mathbf{r},\mathbf{r}_{\rm E},\omega)$ defined by the general relation [6]

$$\mathbf{E}^{\rm sc}(\mathbf{r}) = \frac{1}{\epsilon_0}\left(\frac{\omega}{c}\right)^2 \mathbb{G}^{\rm sc}(\mathbf{r},\mathbf{r}_{\rm E},\omega)\boldsymbol{\mu}_{\rm E}, \tag{12}$$

with $\mathbf{r}_{\rm E} = \underbrace{(R_2+z_{\rm E})}_{r_{\rm E}}\hat{\mathbf{z}}$ being the position of the quantum emitter measured from the origin of coordinates (center of the sphere with radius R_2 in the left panel of Fig. I).

III. ANALYTICAL EXPRESSION FOR THE SPECTRAL DENSITY

We now present a succinct derivation of Eqs. (2)-(4) presented in the main text. The spectral density of the plasmonic gap cavity coupled to the exciton can be computed from the expression of the scattered EM Green's function evaluated at the position of quantum emitter, $\mathbb{G}^{\rm sc}(\mathbf{r}_{\rm E},\mathbf{r}_{\rm E},\omega)$ as

$$J(\omega) = \frac{\Gamma_0(\omega)}{2\pi}\left[1 + \frac{6\pi c}{\omega}\mathrm{Im}\,\mathbb{G}^{sc}_{zz}(\mathbf{r}_{\rm E},\mathbf{r}_{\rm E},\omega)\right], \tag{13}$$

where $\Gamma_0(\omega)$ is the spontaneous emission rate in vacuum at frequency ω. Going back to Eq. (12) and recalling that $\boldsymbol{\mu}_{\rm E} = \mu_{\rm E}\hat{\mathbf{z}}$ we easily see that the crucial step in the analytical calculation of the spectral density is the evaluation of the imaginary part of the $\hat{\mathbf{z}}$ component of the scattered electric field. In the original frame, this component is formally expressed as

$$E_z^{\rm sc}(\mathbf{r}) = \sum_{\alpha'}\left[\mathbb{J}_{\mathbf{r}}\mathbb{O}_{\mathbf{r}'(\mathbf{r})}\right]_{z,\alpha'} E^{'\,\rm sc}_{\alpha'}(\mathbf{r}')\Big|_{\mathbf{r}'=\mathbf{r}'(\mathbf{r})}, \tag{14}$$

where $\mathbb{J}_{\mathbf{r}}$ has matrix elements $(\mathbb{J}_{\mathbf{r}})_{\alpha',\alpha} = \partial\mathbf{r}'_{\alpha'}/\partial\mathbf{r}_{\alpha}$ and $\mathbb{O}_{\mathbf{r}'}$ is the matrix

$$\mathbb{O}_{\mathbf{r}'} := \begin{pmatrix} \frac{x'}{r'} & \frac{x'z'}{\varrho' r'} & -\frac{y'}{\varrho'} \\ \frac{y'}{r'} & \frac{y'z'}{\varrho' r'} & \frac{x'}{\varrho'} \\ \frac{z'}{r'} & -\frac{\varrho'}{r'} & 0 \end{pmatrix}, \tag{15}$$

which still has to be transformed back to the original coordinate frame by using the inverse transformation, $\mathcal{J}$. Here we remind that $\mathbf{r}' = (\boldsymbol{\varrho}', z')$, $\varrho' = \sqrt{x'^2+y'^2}$ and $r' = \sqrt{\varrho'^2+z'^2}$.

To obtain physical insight, it very is natural to consider a *small gap approximation* for which $\delta \ll R_1, R_2$. This is obviously a limiting case but it allows to capture very well the strong coupling physics in the near and extreme near field regime. Under the assumption of small gap-to-radius ratio, it can be shown that the diagonal matrix elements belonging to the blocks $\mathbb{T}_{ij}$ (with $i \neq j$ and $i,j \in \{1,2\}$) present vanishing terms since $r_i^{'\,2} - 1 \to 0$ (note that this actually takes place in the transformed frame). As a consequence, the $\mathbb{R}$ matrix can be proved to present diagonal blocks with matrix elements

$$\mathbb{R}_{ij}(l,l') \simeq \left[\delta_{i,j} - (1-\delta_{i,j})\,\mathrm{e}^{\alpha(\omega)}\left[\frac{1+(i-j)\tilde{\Delta}_i}{1+\tilde{\Delta}_1}\right]^{(i-j)(2l+1)}\right] f_l\left(\frac{1+\tilde{\Delta}_2}{1-\tilde{\Delta}_1},\omega\right)\delta_{l,l'}, \tag{16}$$

and

$$f_l(r,\omega) := \frac{1}{\mathrm{e}^{2\alpha(\omega)}r^{2l+1}-1}. \tag{17}$$

When the relevant energies associated to the exciton are close to those of the localized surface plasmon-polariton resonances and $\gamma \ll \omega$, we can work in the so-called *high-quality resonator limit* [7] which allows us to express the spectral density as a sum of Lorentzian modes $J(\omega) \simeq \sum_{l=0}^{+\infty} \sum_{\sigma=\pm 1} J_{l,\sigma}(\omega)$ with

$$J_{l,\sigma}(\omega) = \frac{g_{l,\sigma}^2}{\pi} \frac{\gamma/2}{(\omega - \omega_{l,\sigma})^2 + (\gamma/2)^2}, \tag{18}$$

similar to the case of the planar metal surface [8] and the single sphere [9]. In the same way, all the surface plasmon-polariton resonances of the nanocavity show the same spectral width controlled by the Drude losses only. The localized surface plasmon-polariton resonant energies depend crucially on the geometrical parameters of the nanostructure, the high-frequency offset and the dielectric background properties, having the following simple functional form

$$\omega_{l,\sigma} = \frac{\omega_{\mathrm{p}}}{\sqrt{\epsilon_\infty + \Omega_{l,\sigma}\epsilon_{\mathrm{D}}}}, \tag{19}$$

with

$$\Omega_{l,\sigma} = \frac{\left(\dfrac{1+\tilde{\Delta}_2}{1-\tilde{\Delta}_1}\right)^{\frac{2l+1}{2}} + \sigma}{\left(\dfrac{1+\tilde{\Delta}_2}{1-\tilde{\Delta}_1}\right)^{\frac{2l+1}{2}} - \sigma}. \tag{20}$$

Importantly, the analytical results show that the exciton placed at the plasmonic gap cavity can be coupled to two different mode families: symmetric modes with resonant energies *lower* than the pseudo-mode energy, $\omega_{l,+} \lesssim \omega_{\mathrm{PS}}$, and antisymmetric modes with resonant energies *larger* than the pseudo-mode energy, $\omega_{l,-} \gtrsim \omega_{\mathrm{PS}}$ [see Fig. 4(a) in the main text]. Furthermore, it can be observed straightforwardly that since $r_{12} := (1+\tilde{\Delta}_2)/(1-\tilde{\Delta}_1) > 1$, $\Omega_{\infty,\sigma} \to 1$ for both symmetric and antisymmetric families. The convergence towards this value is very fast since the function $\Omega_{l,\sigma}$ has a power law dependence on the orbital angular momentum l. In this limit, all the resonances are localized at the surface plasmon-polariton asymptotic frequency characteristic of the Drude metal

$$\omega_{\infty,\pm} = \frac{\omega_{\mathrm{p}}}{\sqrt{\epsilon_\infty + \epsilon_{\mathrm{D}}}}, \tag{21}$$

the latter being roughly equal to the pseudomode frequency $\omega_{\mathrm{PS}} \lesssim \omega_\infty$ for very small gaps.

The coherent coupling factors $g_{l,\sigma}^2 = g_{l,\sigma}^2(\mu_{\mathrm{E}}, z_E, R_1, R_2, \delta)$ between the exciton and the localized surface plasmon-polaritons can be expressed in compact form as

$$g_{l,\sigma}^2 = \frac{\mu_{\mathrm{E}}^2 \omega_{\mathrm{p}}}{4\pi\epsilon_0 \hbar \Delta^3} \left(\frac{\omega_{l,\sigma}}{\omega_{\mathrm{p}}}\right)^3 \frac{\sigma}{2} \frac{\zeta^4}{1-\zeta} \eta_{l,\sigma}^{+} \chi_l(-\zeta)\chi_{l+1}(\zeta)\Big[1 + \mathcal{C}_{l,\sigma}(\zeta, \tilde{\Delta}_1, \tilde{\Delta}_2)\Big], \tag{22}$$

with

$$\mathcal{C}_{l,\sigma}(\zeta, \tilde{\Delta}_1, \tilde{\Delta}_2) := \frac{1}{2}\frac{\eta_{l,\sigma}^{-}}{\eta_{l,\sigma}^{+}} \left[\left(\frac{1-\tilde{\Delta}_1}{1+\tilde{\Delta}_1}\right)^{-(2l+1)} |1-\zeta|^{2l+1} \frac{\chi_l(-\zeta)}{\chi_{l+1}(\zeta)} + \left(\frac{1+\tilde{\Delta}_2}{1+\tilde{\Delta}_1}\right)^{2l+1} |1-\zeta|^{-(2l+1)} \frac{\chi_{l+1}(\zeta)}{\chi_l(-\zeta)} \right]. \tag{23}$$

Here, we have defined the reduced parameters

$$\chi_l(\zeta) := 1 + \frac{l\zeta}{1-\zeta}, \tag{24a}$$

$$\zeta := \frac{\Delta}{r_{\mathrm{E}} - z_0}, \tag{24b}$$

$$\eta_{l,\sigma}^{\pm} := \frac{(1\pm 1)\left(\dfrac{1+\tilde{\Delta}_2}{1-\tilde{\Delta}_1}\right)^{\frac{2l+1}{2}} - \sigma(1\mp 1)}{\left[\left(\dfrac{1+\tilde{\Delta}_2}{1-\tilde{\Delta}_1}\right)^{\frac{2l+1}{2}} - \sigma\right]^2}, \tag{24c}$$

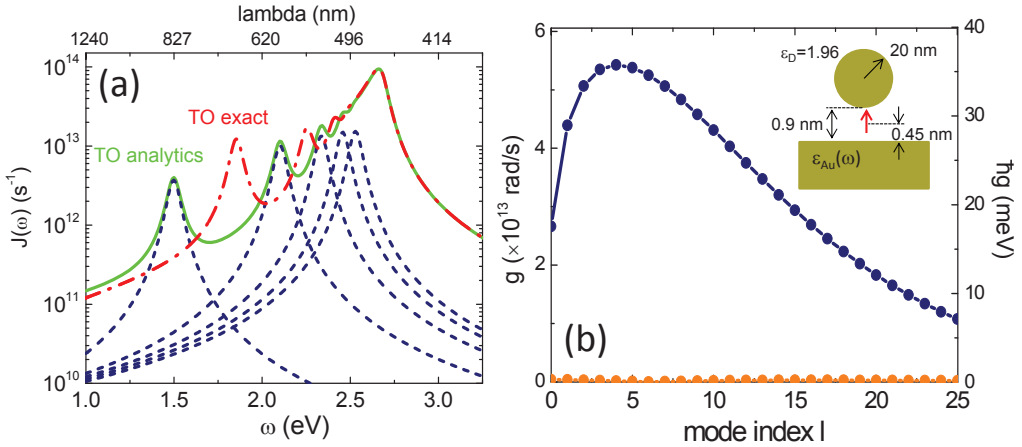

FIG. II: (a) TO exact (red dashed-dotted line) and analytical (green solid line) spectral density for the geometry modelling the experimental samples in Ref. 10 [see inset of panel (a)]. Dark blue dashed lines plot the 5 lowest terms in the Lorentzian decomposition of the analytical $J(\omega)$. (b) Coupling constants for the various even (dark blue) and odd (orange) SP modes contributing to the spectral density in panel(a). As expected (see main text), the contribution due to odd modes is negligible.

and introduced the length governing the volume scaling of the spectral density

$$\Delta := \frac{2(\delta + d)}{1 + \tilde{\Delta}_1}. \tag{25}$$

The structure of the coherent coupling factors given in Eq. (22) admits the following interpretation. The first part is associated with the diagonal blocks of the reflection matrix, $\mathbb{R}_{ij}\delta_{ij}$. As such, we can interpret this term as being the contribution to the scattered field from the two independent spheres. The term $\mathcal{C}_{l,\sigma}(\zeta, \tilde{\Delta}_1, \tilde{\Delta}_2)$ is a consequence of the non-trivial off-diagonal blocks in the reflection matrix, $\mathbb{R}_{ij}(1 - \delta_{ij})$. Therefore, it describes a *cooperative effect* between the two nanospheres due to the presence of the quantum emitter, which manifests in the spectral density. To support this interpretation, we note that both contributions have necessarily to vanish for $l \to +\infty$, $\eta^{\pm}_{\infty,\sigma} \to 0$ (essentially, for convergence reasons). However, the $-$ term, $\eta^{-}_{l\to+\infty,\sigma} \sim r_{12}^{-l}$, vanishes much faster than the $+$ term, $\eta^{+}_{l\to+\infty,\sigma} \sim 2r_{12}^{-l/2}$. Since for higher orbital angular momenta only the strongly localized SPs survive, the contribution due to $\mathcal{C}_{l,\sigma}(\zeta, \tilde{\Delta}_1, \tilde{\Delta}_2)$ has to represent the plasmonic hybridization across the gap of the nanocavity.

IV. COUPLING STRENGTH CALCULATION FOR NATURE 535, 127 (2016)

In this section, we apply our TO approach for the calculation of the exciton-plasmon coupling strength corresponding to the different SP modes supported for the experimental sample in Ref. 10. Mimicking the experimental conditions, we consider a sphere with $R_2 = 20$ nm separated from a flat surface ($R_1 \gg R_2$) by a $\delta = 0.9$ nm gap. The background permittivity is set to $\epsilon_{\rm D} = 1.96$, and the gold permittivity is described through a Drude model with $\epsilon_\infty = 9.7$, $\omega_{\rm p} = 8.91$ eV and $\gamma = 0.08$ eV (parameters taken from Ref. [11]). The QE, placed at the gap center, is modelled through a dipole source with $\mu_{\rm E} = 3.8$ D $= 0.079$ e $\cdot$ nm. Note that $\mu_{\rm E}^2/R_2^3$, $z_{\rm E}/\delta$ and δ/R_2 (all magnitudes that play a key role in $J(\omega)$, see main text) are very similar to those considered in Figure 4(d).

Figure II(a) plots the spectral density for the system above, obtained from both exact (red dashed-dotted line) and analytical (green solid line) TO calculations. The 5 lowest terms in the Lorentzian decomposition of the latter are also shown in dark blue dashed lines. Note that these correspond to even modes (due to the central position of the emitter, the contribution of odd SPs to $J(\omega)$ is negligible, see main text). The exact TO spectrum overlaps with $J(\omega)$ obtained from full EM simulations (not shown here). This is due to the fact that, contrary to the cavity considered in Figure 4 of the main text, the quasi-static approximation is very accurate for the experimental (nanometric-sized) geometry in Ref. [10]. The spectral density presents a dipolar SP maximum at 1.85 eV (670 nm), in very good agreement with experiments, 665 nm. Our calculations yield a Purcell factor equal to $4.3 \cdot 10^6$ for this SP resonance, a value which is also in accordance with measurements ($3.5 \cdot 10^6$). As discussed in the main text, the small gap approximation inherent to our analytical TO approach, leads to red-shifted spectral density maxima at low frequencies. Thus, the analytical dipole SP peak in Figure II(a) emerges at 1.5 eV (827 nm), and the corresponding Purcell enhancement is $3 \cdot 10^6$.

Figure II(b) renders the coupling constants, $g_{l,\sigma}$, versus mode index l, for the different SP modes contributing to the spectra in panel (a). Even and odd modes are rendered in dark blue and orange dots, respectively. As anticipated, the coupling strength for odd SPs is negligible. Note that the coupling constants are obtained for the analytical $J(\omega)$. For the lowest, dipolar, SP mode, we obtain $g_{0,+1} = 19$ meV. A Lorentzian fitting to the corresponding maxima for exact calculations yields $g_{\rm dip}^{\rm fit} = 36$ meV. The difference between these two theoretical results (~ 20 meV) originates from the inherent inaccuracy of the analytical approximation for the lowest SP modes [see for instance Fig. 4 (a) in the main text or Fig. II (a) in this document]. The theoretical value is still in discrepancy with the measured one, $g_{\rm exp} = 90$ meV. In the following, we explore if we can gain insight into this deviation of our predictions from the experimental results.

Our theoretical findings (see main text) indicate that dark, higher multipolar SP modes play a key role in plasmon-exciton coupling in gap nanocavities. We can estimate the coupling strength corresponding to the pseudomode apparent in Figure II(a) at 2.65 eV (470 nm). Exploiting that it results from the spectral overlapping of multiple SPs, we can write [9]

$$g_{\rm PS}^{\rm eff} = \sqrt{\sum_{l\in{\rm PS}}\sum_{\sigma=\pm1} g_{l,\sigma}^2} = \sqrt{\sum_{l=2} g_{l,+1}^2}, \tag{26}$$

where we have dropped the vanishing contribution due to odd SPs, and we have excluded the dipole ($l = 0$) and quadrupole ($l = 1$) modes, as they give rise to clearly discernible peaks in $J(\omega)$. Equation (26) yields $g_{\rm PS}^{\rm eff} = 120$ meV, a prediction very similar to the result obtained from the Lorentzian fitting to the pseoudomode, $g_{\rm PS}^{\rm fit} = 122$ meV. These two values are in much better agreement with experiments, as the discrepancy with respect to $g_{\rm exp}$ has been reduced by a factor of 2. This is a remarkable result, given that our theoretical approach omits experimental aspects such as the impact of inter-band transitions in gold permittivity, the inhomogeneous character of the background dielectric constant, the presence of surface roughness in the nanocavity boundaries, or the uncertainty in the QE position within the gap. We believe that our findings do not only prove the predictive value of our TO-inspired theory, but they also indicate that multipolar SPs (of order higher than dipolar modes) may also have a relevant contribution to the single molecule plasmon-exciton strong coupling reported in Ref. [10].

[1] J. B. Pendry, A. Aubry, D. R. Smith, and S. A. Maier, Science **337**, 549 (2012).
[2] J. B. Pendry, Y. Luo, and R. Zhao, Science **348**, 521 (2015).
[3] L. D. Landau and E. M. Lifshitz, *Electrodynamics of Continous Media* (Pergamon Press, Moscow, 1960).
[4] J. B. Pendry, A. I. Fernández-Domínguez, Y. Luo, and R. Zhao, Nat. Physics **9**, 518 (2013).
[5] R. Zhao, Y. Luo, A. I. Fernández-Domínguez, and J. B. Pendry, Phys. Rev. Lett. **111**, 033602 (2013).
[6] L. Novotny and B. Hecht, *Principles of Nano-Optics* (Cambridge University Press, Cambridge 2012).
[7] E. Waks and D. Sridharan, Phys. Rev. A **82**, 043845 (2010).
[8] A. González-Tudela, P. A. Huidobro, L. Martín-Moreno, C. Tejedor, and F. J. García-Vidal, Phys. Rev. B **89**, 041402(R) (2014).
[9] A. Delga, J. Feist, J. Bravo-Abad, and F. J. García-Vidal, Phys. Rev. Lett. **112**, 253601 (2014).
[10] R. Chikkaraddy, B. de Nijs, F. Benz, S. J. Barrow, O. A. Scherman, E. Rosta, A. Demetriadou, P. Fox, O. Hess, and J. J. Baumberg, Nature **535**, 127 (2016).
[11] A. Vial, A.-S. Grimault, D. Macías, D. Barchiesi,and M. Lamy de la Chapelle, Phys. Rev. B **71**, 085416 (2005).